Coseismic deformation revealed by inversion of strong motion and GPS data: the 2003 Chengkung earthquake in eastern Taiwan

J.-C. Hu, L.-W. Cheng, H.-Y. Chen, Y.-M. Wu, J.-C. Lee, Y.-G. Chen, K.-C. Lin, R.-J. Rau, K. Hao, H.-H. Chen, et al.

Geophys. J. Int. (2007) **169,** 667–674 doi: 10.1111/j.1365-246X.2007.03359.x

Coseismic deformation revealed by inversion of strong motion and GPS data: the 2003 Chengkung earthquake in eastern Taiwan

Jyr-Ching Hu,[1] Li-Wei Cheng,[1] Horng-Yue Chen,[2] Yih-Min Wu,[1] Jian-Cheng Lee,[2] Yue-Gau Chen,[1] Kuan-Chuan Lin,[3] Ruey-Juin Rau,[4] Hao Kuochen,[3] Hui-Hsuan Chen,[4] Shui-Bei Yu[2] and Jacques Angelier[5]

[1] *Department of Geosciences, National Taiwan University, Taipei, Taiwan. E-mail: jchu@ntu.edu.tw*
[2] *Institute of Earth Sciences, Academia Sinica, Nankang, Taiwan*
[3] *Central Weather Bureau, Taipei, Taiwan*
[4] *Department of Earth Sciences, National Cheng Kung University, Tainan, Taiwan*
[5] *Observatoire Océanologique de Villefranche, Géosciences Azur, Villefranche-sur-Mer, France*

Accepted 2007 January 15. Received 2007 January 15; in original form 2005 July 5

SUMMARY

A moderate earthquake of $M_w = 6.8$ occurred on 2003 December 10. It ruptured the Chihshang Fault in eastern Taiwan which is the most active segment of the Longitudinal fault as a plate suture fault between the Luzon arc of the Philippine Sea plate and the Eurasian plate. The largest coseismic displacements were 13 cm (horizontal) and 26 cm (vertical). We analyse 40 strong motion and 91 GPS data to model the fault geometry and coseismic dislocations. The most realistic shape of the Chihshang fault surface is listric in type. The dipping angle of the seismic zone is steep (about 60°–70°) at depths shallower than 10 km and then gradually decreases to 40°–50° at depths of 20–30 km. Thus the polygonal elements in Poly3D are well suited for modelling complex surfaces with curving boundaries. Using the strong motion data, the displacement reaches 1.2 m dip-slip on the Chihshang Fault and decreases to 0.1 m near surface. The slip averages 0.34 m, releasing a scalar moment of 1.6E26 dyne-cm. For GPS data, our model reveals that the maximal dislocation is 1.8 m dip-slip. The dislocations decrease to 0.1 m near the surface. The average slip is 0.48 m, giving a scalar moment of 2.2E26 dyne-cm. Regarding post-seismic deformation, a displacements of 0.5 m were observed near the Chihshang Fault, indicating the strain had not been totally released, as a probable result of near-surface locking of the fault zone.

Key words: Chengkung earthquake, Chihshang fault, coseimic deformation, Taiwan.

INTRODUCTION

The Chengkung earthquake of magnitude $M_w = 6.8$ occurred on 2003 December 10 close to the eastern coast of Taiwan (Fig. 1). The main shock was felt throughout the Taiwan Island. This event did not cause human loss, but significant cracks developed at the ground surface and damaged some buildings. The main surface rupture was located along the western side of the Coastal Range (Lee *et al.* 2006). The hypocentre was first located at 23.106°N–121.324°E at 16 km depth near the town of Chengkung (Kuochen *et al.* 2004). Based on waveform inversion of broad-band seismograms, it was then relocated at 25 km depth by the Broadband Array in Taiwan for Seismology (BATS) (Official BATS website). The location in the deep crust is consistent with a SE-dipping seismic zone, as confirmed by hundreds of aftershocks (Fig. 2). The most realistic shape of the fault surface is listric in type. The dipping angle of the seismic zone is steep (about 60°–70°) at depths shallower than 10 km and then gradually decreases to 40°–50° at depths of 20–30 km. These dips of the seismic zone are consistent with the fault plane solution of the main shock determined through the CMT inversion of broad-band waveforms recorded by the BATS network. These results are consistent with those obtained Kuochen *et al.* (2004, 2007), who combined hypocentre and fault plane solutions of more than 20 aftershocks to reveal that the earthquake occurred on a about 50° east dipping fault (Fig. 2).

The focal mechanism solution obtained with the Finite Dimension Source Model method (FDSM) shows a nearly pure thrust event with minor left-lateral component (Strike = 37°, dip = 50° and rake = 94°). This result has similar dip but slightly different strike and rake than the Harvard CMT solution (strike = 10°, dip = 51° and rake = 69°). Two significant foreshocks occurred about 4 d ($M_L = 5.1$) and 6 min ($M_L = 4.1$) before the main shock. According to Lin (2004), foreshock sequences have repeatedly been observed in this thrust fault system based on the observation of six larger earthquakes ($M_L \geq 5$) since 1992, which had foreshocks at a distance of few kilometres within few days before main shocks.

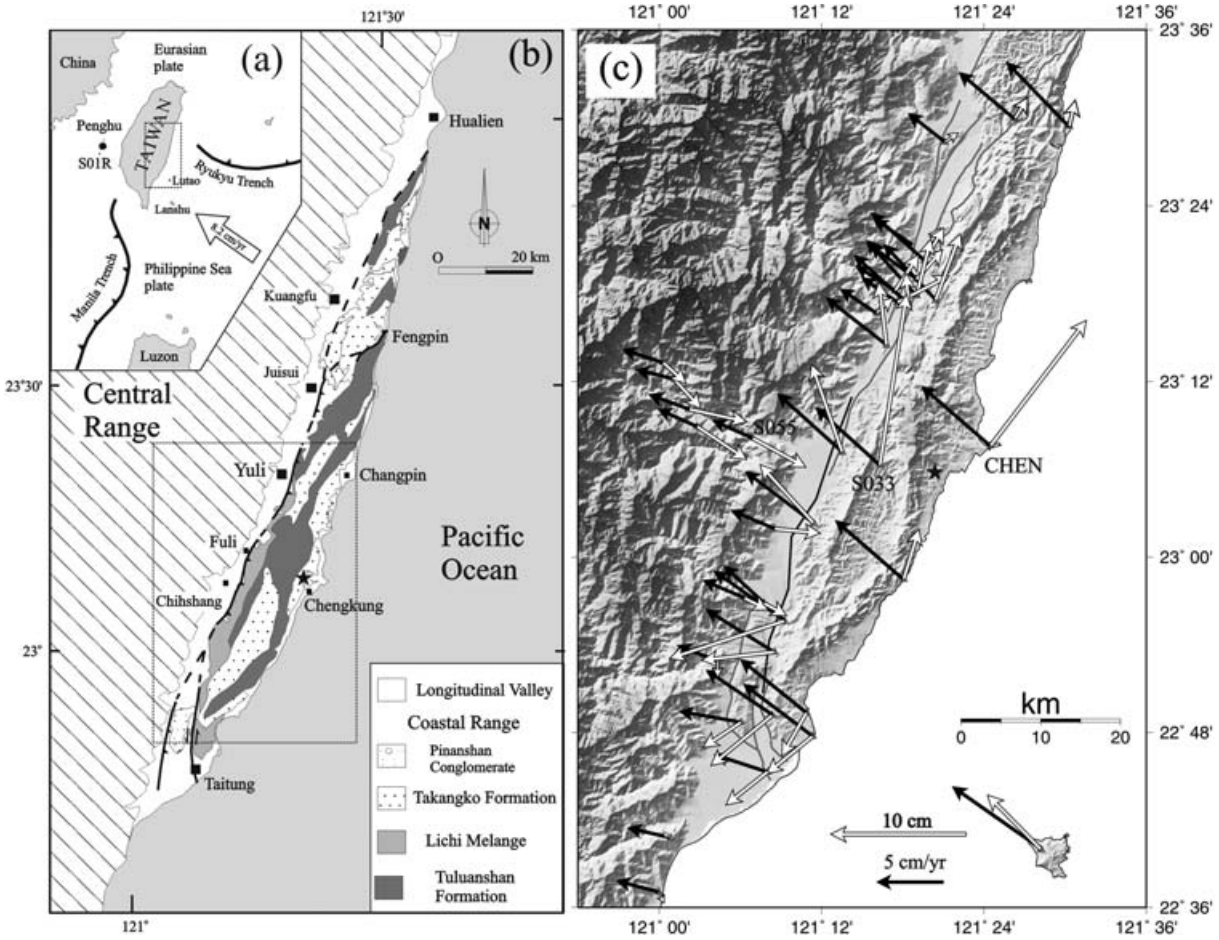

Figure 1. Geodynamic framework and general geological map of the Coastal Range, eastern Taiwan. Solid star: epicentre of Chengkung earthquake. (a) Convergence between Philippine Sea plate and Eurasian plate in Taiwan region. Open arrow: relative motion across Taiwan island, 8.2 cm yr^{-1} towards N309°E (Yu *et al.* 1997, 1999). (b) Simplified geological map of eastern Taiwan. Thick solid and dashed lines: longitudinal Valley Fault (LVF). (c) Velocity field (black arrows) of interseismic period (Yu & Kuo 2001), based on GPS observations from 1992 to 1999 and observed coseismic displacements of the Chengkung Earthquake (white arrows), all with respect to Paisha Station Penghu Islands.

The Chihshang Fault is one of the most active segment of the Longitudinal Valley Fault (LVF). The LVF a plate suture fault between the Luzon arc of the Philippine Sea plate and the Chinese continental margin of the Eurasian plate, in eastern Taiwan (Fig. 1). Annual surveys along the Chihshang Fault during the period 1990–1997 showed a rather constant slip velocity of 2.2 cm yr^{-1} in a N40°W direction, which accommodates 24 per cent of the total contraction across the Taiwan collision belt (Angelier *et al.* 2000; Yu & Kuo 2001; Lee *et al.* 2003). Geological and geodetic surveys showed that the Chihshang Fault is a thrust fault with left-lateral component, involving fault-perpendicular horizontal shortening of nearly 1.7 cm yr^{-1} and fault-parallel slip of 1.4 cm yr^{-1} (Angelier *et al.* 1997, 2000). Despite this high slip rate, the Chihshang Fault experienced slip during minor earthquakes since the last major rupture of the eastern Taiwan earthquake sequence in 1951 ($M_s = 7.1$), until the Chengkung earthquake in 2003 ($M_w = 6.8$). Thus, the behaviour of the Chihshang Fault is complex and combines aseismic creep and earthquake slip.

To determine the displacements related to the Chengkung earthquake, we used both the digital strong-motion seismograph network (40 stations) and 91 GPS stations. The data sets revealed a large contrast in orientation distribution between the interseismic and coseismic stages (Fig. 1c). Whereas the surface displacement vectors of the interseismic period show consistent NW trends (with respect to the Chinese shelf), the coseismic pattern shows surface displacements towards the NNE at the northern end of the fault trace and towards the SW at its southern tip. Only the displacements near the central segment of the rupture trace are NW-directed. In other words, the coseismic displacement pattern is fan-shaped, with edge vectors nearly perpendicular to interseismic ones. Still larger displacements were observed inside the Coastal Range and along the eastern coast (Fig. 1c). The coseismic uplift was maximum (26.3 cm) in the Costal Range. Remarkably, not only were the stations on the hanging wall of the Chihshang Fault uplifted during this earthquake, but also the stations in the Longitudinal Valley and the eastern flank of the Central Range experienced the coseismic uplift.

In this study, we aim at characterizing the kinematic and mechanical behaviour of the Chihshang Fault in light of the Chengkung earthquake, taking into account the measurements of permanent displacement as well as other constraints through inversion and dislocation modelling, assuming that dislocations in homogeneous elastic half-space represent a good approximation of the earthquake faulting.

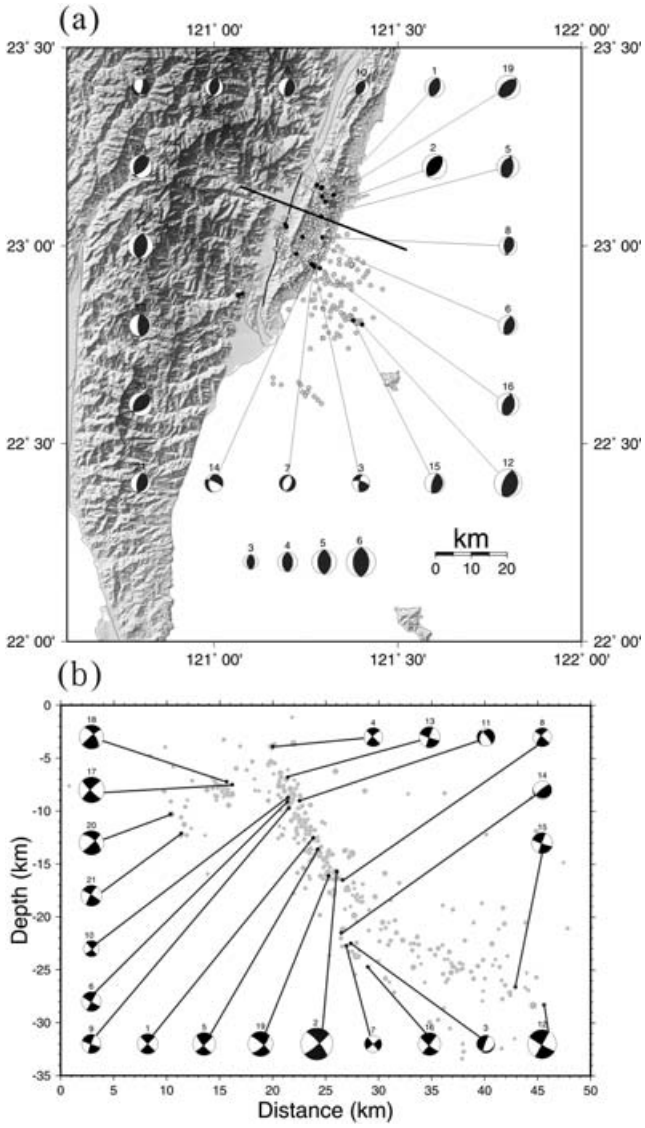

Figure 2. (a) Locations and focal mechanisms of main shock (solid star) and aftershocks of the 2003 December 10 Chengkung earthquake sequence. (b) Projections of foci and focal mechanisms of main shock and major aftershocks (back-wall hemisphere) in the vertical profile located as solid line A–A' in (a).

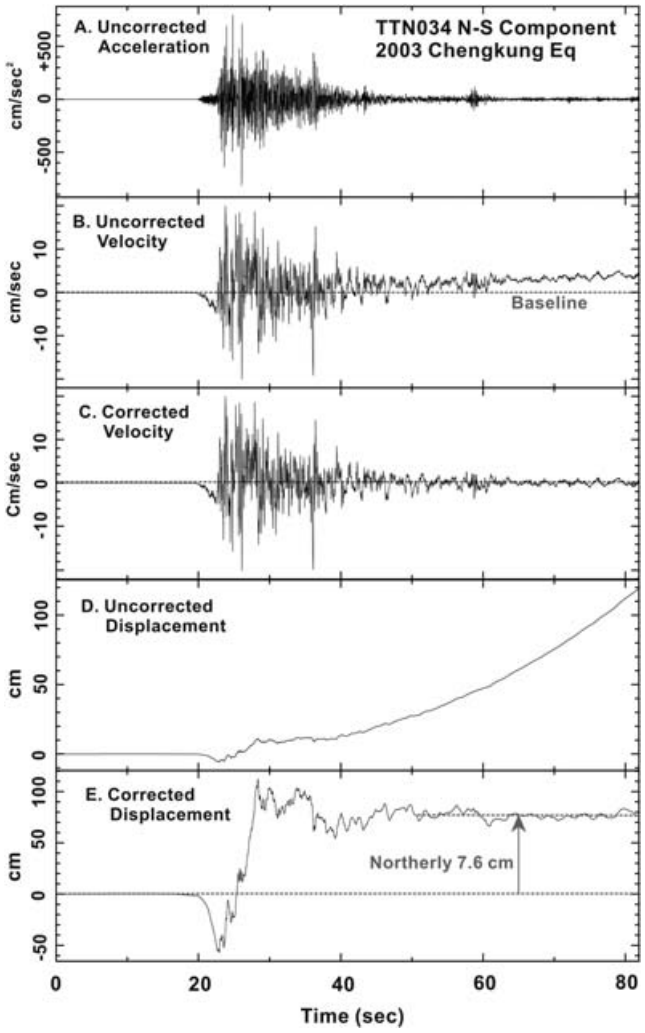

Figure 3. The procedure for conversion of a strong-motion record into site displacement. (a) Original accelerograph record; (b) Uncorrected velocity; (c) Corrected velocity; (d) Uncorrected displacement and (e) Corrected displacement after baseline corrections.

DATA COLLECTIONS AND RESULTS

The Chengkung earthquake triggered many strong motion stations of the Taiwan Strong Motion Instrumentation Program (TSMIP) deployed by the Central Weather Bureau (Wu *et al.* 2006). Provided that appropriate instrument calibration and baseline correction are done, the double integration of the strong ground motion data can yield the permanent displacement. The TSMIP stations are usually operated under low-gain mode. With about 650 modern digital accelerographs installed at free-field sites, their signals are digitized at 200 samples per second or higher at a resolution of 16-bit. Since most accelerographs have clipping level of ± 2 g, it provides us with on-scale records for all near-source strong-motion waveforms. Furthermore, the displacement of the station site itself can be determined after a double integration, provided necessary baseline corrections are correctly done (Chung & Shin 1999; Boore 2001). Thirty-eight stations adjacent to the Chengkung epicentre give a very good picture of the coseismic ground displacement field. The motion shown in Fig. 3(a) was obtained after subtracting the entire acceleration trace by the pre-event interval on the acceleration trace and then integrating once for velocity (Figs 3b and c) and twice for displacement (Figs 3d and e). The non-linear baseline of the acceleration and trend in velocity indicate that ground tilt occurred during the earthquake (Chung & Shin 1999; Boore 2001). We reconstructed the linear trend in velocity and then reintegrated the displacements for all of 40 stations. For example, the corrected seismograms of the north–south component of TTN034 give a coseismic northward displacement of 7.6 cm (Fig. 3e). Judging the qualities of the accelerographs used in this study, the general standard error is about 0.26 cm.

In this study, we calculated 120 coseismic displacements from 40 TSMIP strong motion records to study the source dislocation model. In the northern subarea (near Chengkung), the results indicate a horizontal displacement toward the NE, increasing from 3–4 cm in the Longitudinal Valley to 7–10 cm in the Coastal Range (Fig. 4a). The largest horizontal displacements reconstructed in the southern subarea (near Taitung) are smaller, 2–3 cm in the SE direction (Fig. 4a). The uplift was largest in the epicentre region, about 18 cm (Fig. 4b).

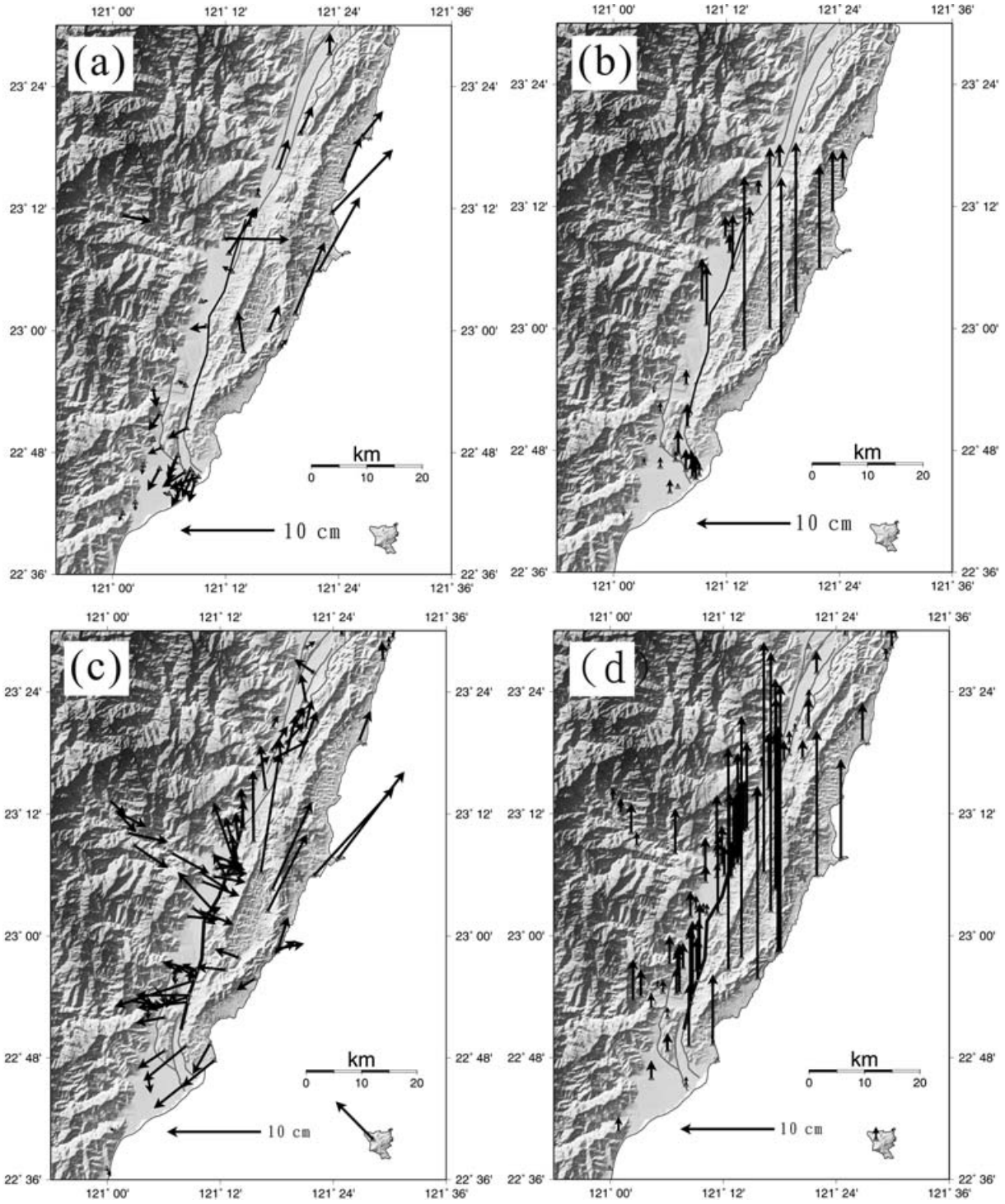

Figure 4. Observed coseismic displacements of the Chengkung earthquake. Solid squares: strong motion stations. Solid triangles: survey-mode GPS stations. Solid circles: continuously recording GPS stations. Solid star: main shock. (a) Horizontal coseismic displacements from strong motion data. (b) Vertical coseismic displacements from strong motion data. (c) Horizontal displacements from GPS data. (d) Vertical displacements from GPS data.

The largest displacements concentrated near the epicentre, which implies a close relationship between crustal movement and main shock rupture.

Nineteen continuously recording GPS stations and more than 86 campaign-mode survey stations have been installed around the study area for monitoring the surface deformation in the southern segment of the LVF. The coseimic displacement was rather well constrained between the daily solutions 344 and 345 of 2003 (the earthquake occurred at UTC 04h 38mn on December 10), according the station position time-series of the continuously recording GPS stations (Chen *et al.* 2006). The data were processed via the standard procedure of the Bernese V4.2 software (Hugentobler *et al.* 2001). The Paisha station (S01R) is located on the stable continental shelf, thus this station was selected to define the minimum constrained

conditions within the International Terrestrial Reference Frame 2000 (ITRF00). The processing procedure is described in detail by Chen *et al.* (2006). To determine the coseismic displacement with the data from the temporary stations, the procedure involved GPS data from days 349 to 354 around the epicentral area. Thus this estimation includes both the coseimic and post-seismic displacements. However, Chen *et al.* (2006) used the preseismic station velocities (2000–2003) to determine the expected station positions on the day of the main shock as well as the correction of nearby continuously recording stations for all campaign-surveyed stations. We thus used the coseismic displacements issued from the data processed by Chen *et al.* (2006), with two additional permanent stations operated by the National Taiwan University.

Significant coseismic displacements have thus been observed (Fig. 4c). On the footwall, that is the LVF and the Central Range, the vectors move towards the N or NNE to the north, the E or ESE in the central area, and SW or SSW to the south. The maximum horizontal coseismic displacement is about 4.5 cm (at station S055). Concerning the hanging-wall, that is the Coastal Range, the coseismic displacements revealed a clear fan-shape with N or NNE trends to the north, NW or W trends in the middle area and SW trends to the south. The maximum horizontal and vertical coseismic displacements near the epicentral area reach about 12.6 and 26.3 cm, respectively (at station S033).

It is worth noting that the patterns of coseismic displacements independently obtained from the strong motion data and the GPS data are quite consistent (compare Figs 4a,b and c,d, respectively). In detail, the results from the GPS indicate a larger shortening across the fault trace in the central subarea (near Chihshang), which could well result from the addition of post-seismic slip during the day of the earthquake (which by definition cannot affect the strong motion data).

INVERSION AND MODELS

We adopted the Poly3D software developed by the Stanford University (Erickson 1986; Thomas 1993) for the inversion of coseismic surface deformation based on the data of strong motions and GPS data. Poly3D evaluates the displacements, strains and stresses induced in an elastic whole- or half-space by planar, polygonal-shaped elements of displacement discontinuity. This numerical code has also been used to model 3-D quasistatic stress distributions around simple or complex fault geometries and the mechanical interactions between faults (Crider & Pollard 1998; Maerten *et al.* 2000; Kattenhorn *et al.* 2001; Soliva *et al.* 2006). Poly3D can derive the displacement and stress fields produced by a triangular element of constant slip by superposing the solution of Comninou & Dundurs (1975) for an angular dislocation. Comninou & Dundurs (1975) extended the solution for an angular dislocation in a whole space (Yoffe 1960) to an elastic half space. The polygonal elements in Poly3D are well suited for modelling complex surfaces with curving boundaries (Maerten *et al.* 2005). Fault surfaces which change in both strike and dip can be meshed by triangular elements without creating gaps or overlaps. Triangular elements are more flexible for simulating complex geometries than the rectangular elements (Okada 1985; Johnson *et al.* 2001). Division of surfaces into triangular elements allows for construction of 3-D fault surfaces that more closely approximate listric surfaces and curved tiplines without introducing overlaps or gaps. We use this benefit of triangular elements to closely fit the surface fault trace, especially the rupturing area around Chihshang.

Displacements $\mathbf{d}^p$ at points (p) on the Earth's surface due to slip $\mathbf{m}^e$ on elements (e) of a buried fault can be described by a set of linear equations

$$d^p = G^{e,p} m^e + E, \tag{1}$$

where $\mathbf{E}$ are the observational errors and $\mathbf{G}^{e,p}$ are the Green's functions, that describe how slip on a fault element produces displacement at the Earth's surface. This set of equations can be used to forward model surface displacements from a known fault geometry and slip distribution, or as an inverse problem to model subsurface fault geometry and slip from an observed set of surface displacements. Inversion for fault geometry is highly non-linear and computationally intensive even for very simple geometries (Cervelli *et al.* 2001). Once the non-linear inversion problem for the geometry of the fault (strike, dip, rake, length, width, etc.) has been solved, the linear inversion (for fixed geometry) is relatively simple since only the linear problem for slip in each fault element has to be solved. Ideally the fault geometry is constrained through integration of multiple data sets such as mapped surface ruptures, high-precision aftershocks locations, reflection seismology, and earthquake focal mechanisms.

To carry out the inverse problem, we search a solution that simultaneously minimizes the L-2 norm of the data misfit and of the model roughness. This method allows fitting of the data to a desired threshold with incorporating the geological concept that slip distributions are somewhat smooth rather than oscillatory (Harris & Segall 1987). As for minimizing the model roughness and misfit, this procedure can prevent overfitting of noisy data and compensates for underdetermined model parameters and geometrical inaccuracies. The misfit and model roughness of the slip inversion can thus be written as:

$$\min\left[\|Gm - d\|_2 + \varepsilon^{-2}\,\|Dm\|_2\right], \tag{2}$$

where $\|Gm\|_2$ is the L-2 norm of the data misfit and $\varepsilon^{-2}\,\|Dm\|_2$ is a measure of the model roughness. The data misfit is calculated by subtracting the observed displacements d form the modelled displacements, which are themselves calculated by multiplying the Green's functions G by the modelled slip m. The model roughness term is composed of a scalar smoothing parameters ε multiplied by the L-2 norm of a discrete second-order difference operator D. This term includes Laplacian of the modelled slip $\nabla^2 m$ in order to minimize the non-dimensional model roughness which is defined as the change in fault slip per length of fault squared (Harris & Segall 1987). The value of ε controls the amount of smoothing and may be smoothing either from a trade-off curve, searching to balance smoothing with data fitting (Harris & Segall 1987). The value of $\varepsilon = 1$ is used for our models.

For understanding the coseismic displacements induced by the Chengkung earthquake, several 3-D dislocation models were used for data inversion. As a first step, we combined the trace of the surface rupture and the distribution of seismicity of the aftershock sequences (Fig. 5) to better constrain the geometry of the Chihshang Fault. Both the surface rupture and the geological mapping show a nearly N20° strike (Lee *et al.* 2006). The relocated seismicity defines a SE-dipping inclined fault zone, listric in type, which extends from the surface to a depth of about 30 km. The fault geometry we employ for the dislocation model, after all, is divided into six segments with different dip angle to delineate the aftershock distribution (Table 1). All layers strike N18°E and change each dip angle, roughly depending on the depth, from 60° at the top to 10° at the end (Fig. 5b). And the top layer is carefully mapped according to the fault trace. The optimal fault has 49 vertices constructing 72 isosceles triangular elements (Fig. 5a). The total measure of area is

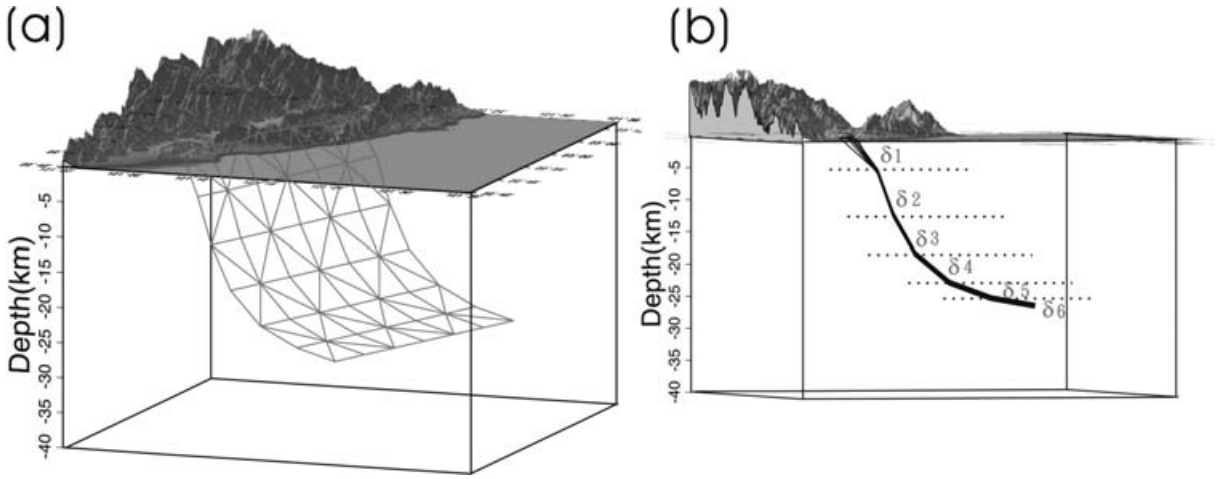

Figure 5. (a) The 3-D fault geometry used in this dislocation model. The optimal fault has 49 vertices constructing 72 isosceles triangular elements. The total measure of area is 1764 km^2. (b) The side view of fault geometry. Each dip angle is selected from Table 1.

1764 km^2. The best-fitting model is estimated by the weighted root mean square described by (Segall & Harris 1986). The misfit for the best model in comparison with geodetic observation is 22.14 mm in E–W, 7.35 mm in N–S and 26.58 mm for vertical component, respectively.

The 3-D dislocation model based on Poly3D code in term of GPS data reveals that the maximal dislocation is about 1.8 m slip and the dislocations decrease to 10 cm near the surface (Fig. 6a). The average slip is 0.48 m along the fault surface, which yields a scalar moment of 2.2×10^{26} dyne-cm. These results are similar to that of the Harvard CMT, indicating a scalar moment of 2.0×10^{26} dyne-cm. The 3-D dislocation model based on strong motion data reveals that the maximal dislocation is about 1.2 m dip-slip on the Chihshang fault and the dislocations decrease to about 10 cm near the surface (Fig. 6b). The average slip is about 0.34 m along the fault surface, which releases a scalar moment of 1.6×10^{26} dyne-cm.

Fig. 6 shows the results of the inversion based on the use of the GPS data. The calculated horizontal coseismic deformation reveals a radial, fan-shaped pattern that well fits the observation for both the strong motion and the GPS data. The gross trend in net slip at the ground surface is quite consistent with those issued from geodetic and strong motion data for both the horizontal deformation (Figs 4a and c, respectively, compare with Fig. 7a) and the vertical displacement (Figs 4b and d, respectively, compare with Fig. 7b).

DISCUSSIONS AND CONCLUSIONS

Because of the large amount of data that constrain the distribution of coseismic motion, the Chengkung earthquake ($M_w = 6.8$, 2003 December 10) provides good access to the mechanical response of the crust during a thrust-type event. In addition, the surface rupture is well documented, because the main shock reactivated the NNE-striking Chihshang Fault (along the suture zone of the Philippine Sea plate and Eurasian plate in eastern Taiwan). The distribution of the shocks tightly constrains the shape of the fault zone in the crust

Table 1. The geometry of delineation of the aftershocks.

	δ_1	δ_2	δ_3	δ_4	δ_5	δ_6
Optimal dip angle	60°	65°	60°	40°	20°	10°

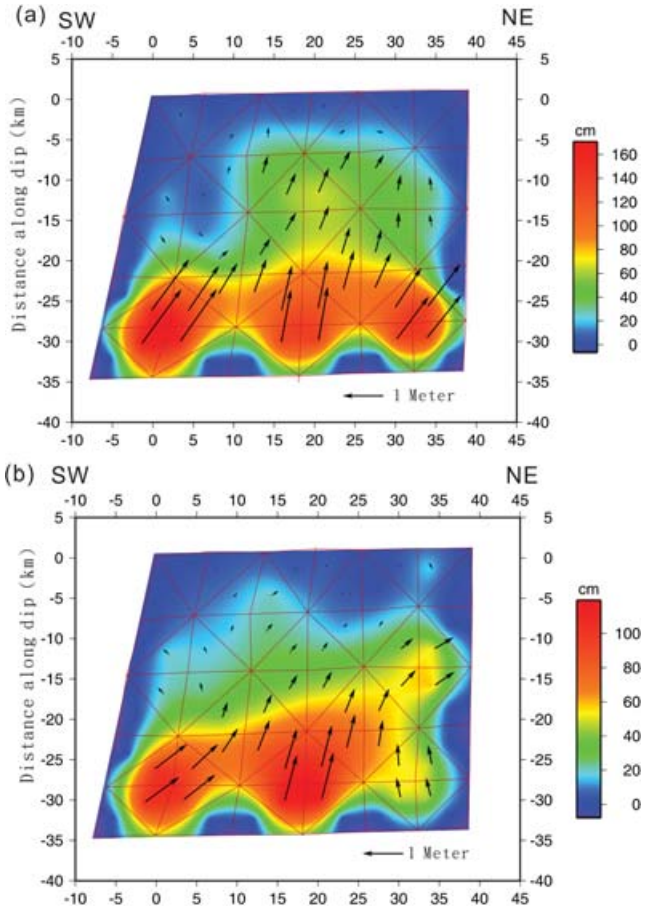

Figure 6. Coseismic slips along the fault surface based on inversion of coseismic displacements. (a) Inversion of GPS data. (b) Inversion of strong motion data.

(Fig. 5). Both the focal mechanisms and the displacement data concur to constrain the fault plane and slip orientations. The largest coseismic displacements were about 13 and 26 cm (horizontal and vertical components, respectively). The large amount of information enabled us to analyse 40 strong motion data and 91 GPS data (permanent and temporary) around the epicentral area and the

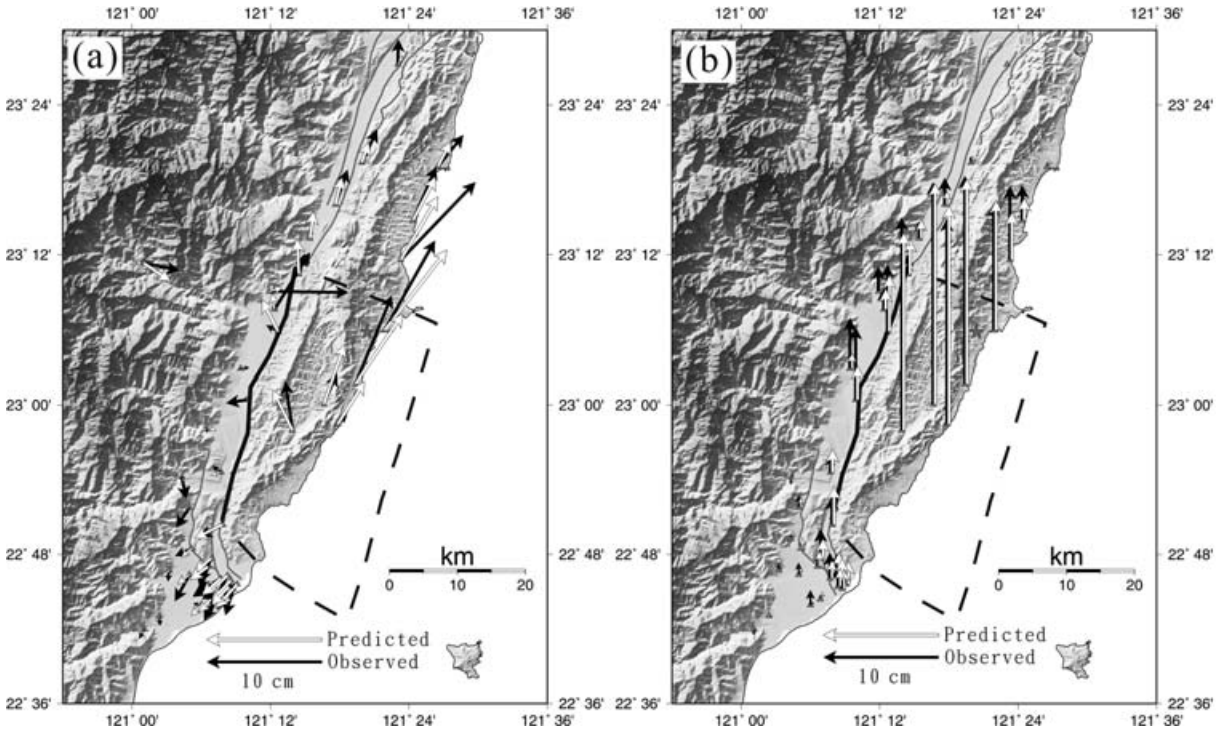

Figure 7. Coseismic displacements calculated at stations from the best-fitting fault model, to be compared with observed displacements obtained at 40 strong motion and six continuous GPS stations. (a) Horizontal displacements. (b) Vertical displacements. Compare with Fig. 4.

Chihshang Fault and thus to constrain the model of fault plane geometry (Fig. 5) and the distribution of coseismic dislocation (Figs 6 and 7).

Our 3-D dislocation model based on Poly3D code in term of strong motion data reveals that the maximal dislocation is about 1.2 m dip-slip on the Chihshang Fault plane and the dislocations decrease to about 0.10 m near the surface, in agreement with the data. The average slip is about 0.34 m along the fault surface, which releases a scalar moment of 1.6×10^{26} dyne-cm. After inversion, the model based on GPS data reveals that the maximal dislocation is about 1.8 m dip-slip at depth while the dislocations decrease to 10 cm near the surface. The average slip is 0.48 m along the fault surface that gives a scalar moment of 2.2×10^{26} dyne-cm, in agreement with the Harvard CMT mechanism that indicated a scalar moment of 2.0×10^{26} dyne-cm.

The modelling results allow us to delineate the seismogenic extent of the Chihshang fault. Interestingly, the shallow part of the fault, which contributed very little to slip during the Chengkung earthquake, experienced significant movement during the month following the earthquake. The dislocation model clearly reveals the location and extent of the major seismogenic source, 20 km and more from the surface along fault dip (Fig. 6). Despite simplification, this 3-D dislocation model well accounts for the actual distribution of the coseismic displacements (compare Figure 6 and white arrows in Fig. 1c). Considering the shape of the fault zone (Fig. 5), this along-dip distance corresponds to depth of 17 km and more: this result well fits the recorded depths of the main shock (16 and 25 km, see earlier description). Also, our dislocation model well accounts for the major contrast between the coseismic and interseismic patterns in terms of horizontal displacement trends (compare Figs 4 and 1c). Our model thus implies that the LVF is segmented at depths larger than 10 km in the Chihshang region.

This mechanical behaviour, which is consistent with the relatively large amount of post-seismic displacement along the fault trace in the months following the earthquake, raises inferences in terms of seismic hazard. To this respect, our modelling is quite consistent with the unexpected results of local geodetic surveys along the Chihshang Fault, which revealed near-surface locking of the fault (Lee *et al.* 2006). These significant post-seismic displacements result from the adjustment of slip along the fault surface in the shallow part of the Chihshang Fault. We conclude that the compressive strain had not been totally released, as a probable consequence of the partial locking that affects the shallow part of the active fault zone.

ACKNOWLEDGMENTS

The authors are grateful to Martin Mai and an anonymous reviewer for constructive comments and suggestions to improve our manuscript. We also thank Chia-Yu Lu, Yu-Chang Chan, Wen-Shan Chen and Hau-Tsu Chu for suggestions and discussions. This research was supported by grants from the National Science Council of Taiwan (NSC 91-2119-M-002-020) and the Central Geological Survey of the MOEA. Some figures were produced using the Generic Mapping Tools written by Paul Wessel and Walter H. F. Smith.

REFERENCES

Angelier, J., Chu, H.-T. & Lee, J.-C., 1997. Shear concentration in a collision zone: kinematics of the active Chihshang fault, Longitudinal Valley, eastern Taiwan, *Tectonophysics*, **274**, 117–144.

Angelier, J., Chu, H.-T., Lee, J.-C. & Hu, J.-C., 2000. Active faulting and earthquake hazard: the case study of continuous monitoring of the of the Chihshang Fault, Taiwan, *J. Geodyn.*, **29**, 151–185.

Boore, D.M., 2001. Effect of baseline corrections on displacement and response spectra for several recodings of the 1999 Chi-Chi, Taiwan, earthquake, *Bull. seism. Soc. Am.*, **91**, 1199–1211.

Cervelli, P., Murray, M., Segall, P., Aoki, Y. & Kato, T., 2001. Estimating source parameters from deformation data, with an application to the March 1997 earthquake swarm off the Izu Peninsula, Japan, *J. geophys. Res.*, **106**, 11 217–11 237.

Chen, H.-Y., Yu, S.-B., Kuo, L.-C. & Liu, C.-C., 2006. Coseismic and postseismic displacement of the 10 December 2003 (Mw 6.5) Chengkung earthquake, eastern Taiwan, *Earth Planets Space*, **58**, 5–21.

Chung, J.K. & Shin, T.C., 1999, Implication of the rupture process from the displacement distribution of strong ground motions recorded during the 21 September 1999 Chi-Chi, Taiwan earthquake, *Terr. Atmos. Ocean. Sci.*, **10**, 777–786.

Comninou, M. & Dundurs, J., 1975. The angular dislocation in a half space, *J. Elasticity*, **5**, 203–216.

Crider, J.G. & Pollard, D.D., 1998. Fault Linkage: Three-dimensional mechanical interaction between echelon normal faults, *J. geophys. Res.,* **103**(B10), 24373–24391.

Erickson, L.L., 1986. A three-dimensional dislocation program with applications to faulting in the earth, *M. S. thesis*, Stanford University, Stanford, California, 167 pp.

Harris, R.A. & Segall, P., 1987. Detection of a locked zone at depth on the Parkfield, California, segment of the San Andreas Fault, *J. geophys. Res.,* **92,** 7945–7962.

Hugentobler, U., Schear, S. & Fridez, P., 2001. Bernese GPS software version 4.2, Astro. Inst. Univ. of Berne, Berne, Switerland, 515 pp.

Johnson, K.M., Hsu, Y.-J., Segall, P. & Yu, S.-B., 2001. Fault geometry and slip distribution of the 1999 Chi-Chi, Taiwan earthquake imaged from inversion of GPS data, *Geophys. Res. Lett.*, **29**, 2285–2288.

Kattenhorn, S.A. & Pollard, D.D., 2001. Integrating 3-D seismic data, field analogs, and mechanical models in the analysis of segmented nornmal faults in the Wytch Farm oil field, southern England, U.K., *AAPG Bull.,* **85,** 1183–1210.

Kuochen, H., Wu, Y.-M. Chang, C.-H., Hu, J.-C. & Chen, W.-S., 2004. Relocation of eastern Taiwan earthquakes and tectonic implications, *Terres. Atmos. Ocean. Sci.*, **15**, 647–666.

Kuochen, H. Wu, Y.-M. Chen Y.-G. & Chen, R.-Y., 2007. 2003 Mw 6.8 Chengkung earthquake and its associated seismogenic structures, *J. Asian Earth Sci.*, doi:10.1016/j.jseaes.2006.07.028.

Lee, J.-C., Angelier, J., Chu, H.-T., Hu, J.-C., Jeng, F.-S. & Rau, R.-J., 2003. Active fault creep variations at Chihshang, Taiwan, revealed by creepmeter monitoring, 1998–2001, *J. geophys. Res.*, **108**(B11), 2528, doi:10.1029/2003JB002349.

Lee, J.-C., Chu, H.-T., Angelier, J., Hu, J.-C., Chen, H.-Y. & Yu, S.-B., 2006. Quantitative analysis of surface coseismic faulting and postseismic creep accompanying the 2003, Mw = 6.5, Chengkung earthquake in eastern Taiwan, *J. geophys. Res.*, **111**, B02405, doi:10.1029/2005JB003612.

Lin, C.-H., 2004. Repeated foreshock sequences in the thrust faulting environment of eastern Taiwan, *Geophys. Res. Lett.*, **31**, L13601, doi: 10.1029/2004GL019833.

Maerten, F., Resor, F., Pollard, D. & Maerten, L., 2005. Inverting for slip on three-dimensional fault structures using angular dislocations, *Bull. seism. Soc. Am.*, **95**, 1654–1665, doi:10.1785/0120030181.

Maerten, L. Pollard, D.D. & Karpuz, R., 2000. How to constrain 3D fault continuity and linkage using reflection seismic data: a geomechanical approach, *AAPG Bull.,* **84,** 1311–1324.

Okada, Y., 1985. Surface deformation due to shear and tensile faults in a half-space, *Bull. seism. Am.*, **75**(4), 1135–1154.

Segall, P. & Harris, R., 1986. Slip deficit on the San Andreas fault at Parkfield, California, as revealed by inversion of geodetic data, *Science*, **23**, 1409–1413.

Soliva, R., Benedicto, A. & Maerten, L., 2006. Spacing and linkage of confined normal faults: importance of mechanical thickness, *J. geophys. Res.*, **111**, B01402, doi:10.1029/2004JB003507.

Thomas, A.L., 1993. Ploy3D: a three-dimensional, polygonal element, displacement discontinuity boundary element computer program with application to fractures, faults and cavities in the Earth's crust, *M.S. thesis*, Stanford University, Stanford, CA, 97 pp.

Wu, Y.-M. *et al.*, 2006. Coseismic versus interseismic ground deformations, fault rupture inversion and segmentation revealed by 2003 Mw 6.8 Chengkung earthaquake in eastern Taiwan, *Geophys. Res. Lett.*, **33**, L02312, doi:10.1029/2005GL024711.

Yoffe, E., 1960. The angular dislocation, *Philosophical Magazine*, **5**, 161–175.

Yu, S.-B., Chen, H.-Y. & Kuo, L.-C., 1997, Velocity field of GPS stations in the Taiwan area, *Tectonophysics*, **274**, 41–59.

Yu, S.-B. & Kuo, L.-C., 2001. Present-day crustal motion along the Longitudinal Valley Fault, eastern Taiwan, *Tectonophysics*, **333**, 199–214.

Yu, S.-B. Kuo, L.-C., Punongbayan, R.S. & Ramos, E.G., 1999. GPS observation of crustal deformation in the Taiwan–Luzon region, *Geophys. Res. Lett.,* **26,** 923–926.